Title

SPIO-labeled Yttrium Microspheres for MR Imaging Quantification of Transcatheter Intrahepatic Delivery in a Rodent Model.

Permalink

https://escholarship.org/uc/item/1516z1pm

Journal

Radiology, 278(2)

ISSN

0033-8419

Authors

Li, Weiguo
Zhang, Zhuoli
Gordon, Andrew C
et al.

Publication Date

2016-02-01

DOI

10.1148/radiol.2015150315

Peer reviewed

Radiology

SPIO-labeled Yttrium Microspheres for MR Imaging Quantification of Transcatheter Intrahepatic Delivery in a Rodent Model[1]

Weiguo Li, PhD
Zhuoli Zhang, MD, PhD
Andrew C. Gordon, BS
Jeane Chen, BS
Jodi Nicolai, MS
Robert J. Lewandowski, MD
Reed A. Omary, MD, MS
Andrew C. Larson, PhD

© RSNA, 2015

Purpose: To investigate the qualitative and quantitative impacts of labeling yttrium microspheres with increasing amounts of superparamagnetic iron oxide (SPIO) material for magnetic resonance (MR) imaging in phantom and rodent models.

Materials and Methods: Animal model studies were approved by the institutional Animal Care and Use Committee. The r2* relaxivity for each of four microsphere SPIO compositions was determined from 32 phantoms constructed with agarose gel and in eight concentrations from each of the four compositions. Intrahepatic transcatheter infusion procedures were performed in rats by using each of the four compositions before MR imaging to visualize distributions within the liver. For quantitative studies, doses of 5, 10, 15, or 20 mg 2% SPIO-labeled yttrium microspheres were infused into 24 rats (six rats per group). MR imaging R2* measurements were used to quantify the dose delivered to each liver. Pearson correlation, analysis of variance, and intraclass correlation analyses were performed to compare MR imaging measurements in phantoms and animal models.

Results: Increased r2* relaxivity was observed with incremental increases of SPIO microsphere content. R2* measurements of the 2% SPIO–labeled yttrium microsphere concentration were well correlated with known phantom concentrations ($R^2 = 1.00$, $P < .001$) over a broader linear range than observed for the other three compositions. Microspheres were heterogeneously distributed within each liver; increasing microsphere SPIO content produced marked signal voids. R2*-based measurements of 2% SPIO–labeled yttrium microsphere delivery were well correlated with infused dose (intraclass correlation coefficient, 0.98; $P < .001$).

Conclusion: MR imaging R2* measurements of yttrium microspheres labeled with 2% SPIO can quantitatively depict in vivo intrahepatic biodistribution in a rat model.

©RSNA, 2015

Online supplemental material is available for this article.

Hepatocellular carcinoma and secondary metastases to the liver are several of the most common malignancies worldwide (1,2). One powerful treatment option for hepatocellular carcinoma and liver metastasis is radioembolization with yttrium 90 (^{90}Y) microspheres (3). Radioembolization involves catheter-directed infusion of glass or resin ^{90}Y microspheres that provide an internal radiation dose to liver tumors. However, heterogeneous intrahepatic biodistribution of these microspheres could potentially lead to suboptimal responses (4,5). Knowledge of the patient-specific distribution of these microspheres may be critical to permit early prediction of treatment response. Visualization and quantification of the heterogeneous biodistribution of ^{90}Y microspheres could guide catheter placement prior to additional infusions and/or elicit adoption of alternative treatment modalities in cases of suboptimal dose delivery.

The current clinical practice to determine the distribution of the microspheres, bremsstrahlung imaging combined with anatomic imaging with single photon emission computed tomography (SPECT)/computed tomography (CT), is not quantitative, and thus accurate

dose distributions cannot be determined (6,7). Technetium-99m macro-aggregated albumin (^{99m}Tc-MAA) particles have served as a surrogate for in vivo prediction of ^{90}Y microsphere biodistribution (8). However, the size differences, along with the fundamental morphology differences between ^{99m}Tc-MAA particles and microspheres and the poor spatial resolution of SPECT studies lead to relatively inaccurate predictions of resulting biodistributions (9). Recent studies have shown that the distribution of ^{90}Y microspheres can also be assessed by using positron emission tomography (PET) or PET/CT (10–12). However, particularly when using clinical PET or PET/CT scanners, these images may not offer sufficient spatial resolution for depiction of intratumoral biodistribution. Furthermore, the lack of soft-tissue contrast within PET images requires fusion of PET with CT data sets to provide requisite anatomic references. Misregistration between PET and CT data sets can represent a potential problem for this dual modality approach.

Labeling ^{90}Y microspheres with superparamagnetic iron oxide (SPIO) offers the potential to use MR imaging to visualize in vivo biodistributions (13). Susceptibility differences between SPIO particles and surrounding tissues lead to local magnetic field gradients with proportional signal losses through R2* relaxation mechanisms. Feasibility studies demonstrated that SPIO-labeled radioembolization microspheres permit qualitative visualization of microsphere biodistribution following transcatheter delivery to the liver (13). However, the strong susceptibility effects of SPIO can rapidly reduce the MR signal below the noise floor, thus complicating quantification procedures. Therefore, optimal selection of the amount of SPIO material included within these microspheres may be critical to permit in vivo quantification

of microsphere delivery to targeted tissues.

In our study, we hypothesized that yttrium microspheres labeled with SPIO would permit in vivo quantification of microsphere delivery to the liver. We investigated the qualitative and quantitative impact of labeling yttrium microspheres with increasing amounts of SPIO material for MR imaging in phantom and rodent models.

Materials and Methods

SPIO-labeled Microspheres

Yttria-alumina-silicate (YAS) microspheres contained SPIO dispersed throughout each glass sphere (added during the manufacturing process) (Mo-Sci Medical, Rolla, Mo). Microspheres containing 2%, 5%, 10%, and 20% SPIO (percentage by mass) with a diameter distribution from 20 to 40 μm were used for this study (13).

Phantom Models

Thirty-two agarose gel phantoms were constructed for each of the four different microsphere compositions to compute the R2* relaxation rates and to evaluate the r2* relaxivity characteristics of the

Advances in Knowledge

- Yttrium microspheres labeled with 2% superparamagnetic iron oxide (SPIO) content showed a high correlation with MR imaging R2* measurements ($R^2 = 1.00$, $P < .001$) over a broad range of concentrations (from 0 to 16 mg/mL).

- MR imaging R2* measurements were in strong agreement with the infused doses of yttrium microspheres labeled with 2% SPIO content (intraclass correlation coefficient, 0.98; $P < .001$) in a rat model at 7.0 T.

- Yttrium microspheres labeled with relatively low SPIO content (2% by mass) permit MR imaging for quantitative depiction of microsphere delivery to liver tissues.

Implication for Patient Care

- Accurate depiction of intrahepatic yttrium 90 microsphere delivery may permit early prediction of treatment response.

YAS microspheres (J.N., with 6 years of experience). Agarose gel was placed within 15-mm-inner-diameter nuclear MR tubes (New Era Enterprises, Vineland, NJ) along with 0, 0.25, 0.5, 1.0, 2.0, 4.0, 8.0, or 16.0 mg/mL samples of SPIO-labeled microspheres (approximately 50000 spheres per milligram). Thus, the maximum concentration for SPIO-labeled microspheres in these phantoms was approximately 800 spheres per cubic millimeter.

Rodent Models

All experiments were approved by the institutional Animal Care and Use Committee and were performed in accordance with Committee guidelines. To investigate the impact of altering yttrium microsphere SPIO content, in vivo and ex vivo comparison studies were performed following transcatheter infusions in a rodent model. Four male Sprague-Dawley rats (Charles River Laboratories, Wilmington, Mass) weighing 200–350 g were used in these experiments. Rats were anesthetized with intramuscular injection of ketamine (75–100 mg per kilogram of body weight) (Ketanest; Parke-Davis, Freiburg, Germany) and xylazine (2–6 mg/kg) (Rompun; Bayer, Leverkusen, Germany). After anesthetization, each rat was catheterized through the portal vein (see below). After catheterization, the animal was scanned with MR imaging. Next, 5 mg of microspheres in 1 mL saline were administered through the catheter. Immediately after MR imaging, rats were euthanized by intraperitoneal injection using 2 mL of Euthasol (Virbac AH, Fort Worth, Tex). Livers were harvested and fixed using 10% buffered formalin for ex vivo MR imaging and histologic analysis. One additional harvested rat liver (infused with microspheres of 5% SPIO content) was imaged to obtain high-resolution T2-weighted images to visualize microsphere deposits in liver tissue (animal model studies were performed by W.L., with 5 years of experience; J.C. and A.C.G., with 4 years of experience; and Z.Z., with > 10 years of experience).

For quantitative measurements of SPIO-labeled yttrium microsphere delivery, 24 adult Sprague-Dawley rats weighing 200–350 g were separated into four groups (six rats per group) receiving transcatheter intrahepatic 1 mL infusions of 5, 10, 15, or 20 mg of 2% SPIO-labeled YAS microspheres in saline, respectively. In vivo MR imaging was performed before and after administration of the microspheres.

YAS Microsphere Infusion

For all rats, skin incisions and dissections were performed to expose the portal vein. Sutures were placed proximal and distal to the intended access point. A 24-gauge catheter (BD, Franklin Lakes, NY) was used to cannulate the portal vein. Once access was obtained, the sutures were used to secure access and achieve hemostasis. The rat was then transferred to the MR imaging bore for preinfusion MR imaging. The transcatheter infusion of YAS microsphere-saline mixture was then performed followed by two 1 mL saline flushes, while the rat was kept in the magnet to minimize pre- and postinfusion misregistration (W.L., with 5 years of experience, and Z.Z., with > 10 years of experience).

MR Imaging

All MR imaging studies were performed by using a 7.0-T 30-cm–bore Bruker ClinScan MR imaging unit (Bruker Biospin MR Imaging, Ettlingen, Germany) with (a) Siemens Syngo clinical user interface and pulse sequences, (b) 75-mm QuadTransceiver rat coil (Bruker Biospin), (c) isoflurane anesthesia system, body temperature control and monitoring system for vital signs (temperature and respiration rates), and (d) MR imaging-compatible small animal gating system (SA Instruments, NY) to permit free-breathing acquisitions during pre- and postinfusion MR imaging measurements (W.L. and Z.L., both with > 10 years of experience in MR imaging).

The phantoms were positioned at the center of the magnet. Careful manual shimming was performed before R2* measurements. Quantitative R2* measurements were obtained by using a multiple–gradient-echo sequence with repetition time msec/echo times msec, 200/2.6, 5.7, 8.8, and 11.9; flip angle, 30°, section thickness, 1 mm; field of view, 65 mm; matrix, 192 × 192; number of excitations, two; and readout bandwidth, 360 Hz/pixel.

For rodent imaging, all studies were synchronized with the respiratory cycle to minimize motion artifacts. The in vivo distribution of SPIO-labeled microspheres was qualitatively characterized with a T2-weighted turbo spin-echo (TSE) sequence, a T1-weighted segmented gradient-echo sequence with an inversion-recovery preparatory pulse, and a proton density–weighted gradient-echo sequence. The T2-weighted TSE sequence was applied with the following parameters: 2920/29; turbo factor, 12; matrix, 264 × 384; field of view, 61 × 90 mm; number of coronal sections, 32; section thickness, 0.7 mm; number of excitations, one; and imaging time, 7 minutes. The proton density–weighted gradient-echo sequence was performed with 15/3.3; flip angle, 5°; matrix, 256 × 178; field of view, 50 × 35 mm; number of coronal sections, 32; section thickness, 0.7 mm; and imaging time, 11 minutes. The T1-weighted inversion-recovery preparatory pulse sequence was applied with 1340/1.84; inversion time, 1200 msec; matrix, 264 × 384; field of view, 61 × 90 mm; number of coronal sections, 32; section thickness, 0.7 mm; number of excitations, one; and imaging time, 14 minutes. In vitro T2-weighted images were acquired at a spatial resolution of 0.12 × 0.12 × 0.12 mm by using a three-dimensional TSE sequence with 2750/46; field of view, 30 × 30 mm; and number of excitations, four. Before and after infusion of the yttrium microspheres, in vivo R2* measurements were performed by using the multiple–gradient-echo sequence with 200/2.6, 5.7, 8.8, and 11.9; flip angle, 30°; field of view, 65 × 60 mm; matrix, 192 × 192; section thickness, 0.7 mm; and readout bandwidth, 360 Hz/pixel.

Histologic Evaluation

Excised livers were fixed in 10% buffered formaldehyde solution overnight. Segments were sliced at 5-mm intervals and embedded in paraffin for histopathologic examination. These segments were sliced in 30-μm-thick slices and

were stained with hematoxylin-eosin to confirm parenchymal delivery of the yttrium microspheres. Histologic slides were digitized by using a multichannel automated imaging system (Tissue Gnostics, Austria), and histopathologic images were examined to determine the location of intrahepatic microsphere deposition (W.L., with 5 years of experience, and J.C. and A.C.G., with 4 years of experience).

Data Analysis

Image postprocessing was performed offline using Matlab software (Math Works, Natick, Mass) (W.L., with > 10 years experience with MR imaging data processing). Relaxation rate R2* maps were calculated voxelwise by using the nonlinear Levenberg-Marquardt algorithm to fit the monoexponential decay component: $S_{TEi} = S_0 \cdot \exp(-R2^* \cdot TEi)$, where S_{TEi} is the MR signal intensity at the echo time TEi and S_0 is the MR signal intensity at echo time 0.

For quantitative analysis in phantoms, a region of interest (ROI) was drawn to encompass the microsphere-infused gel portion of each phantom in the R2* maps. Identical ROI sizes were used for each phantom measurement. For each composition of yttrium microspheres, the measured R2* values were fit to a linear regression model to extract the r2* relaxivity with the following equation:

$$R2^*(i) = R2^*(0) + r2^* \cdot [SPIO](i), \quad (1)$$

where R2*(i) is the R2* value measured at the ith of the eight concentrations of SPIO, R2*(0) was determined from gels without SPIO-labeled microspheres, and [SPIO](i) is the ith concentration of SPIO-labeled yttrium microspheres in milligrams per millimeter.

For the quantitative animal model studies, yttrium microsphere concentration maps were generated from voxelwise R2* maps and Eq (1) with a baseline offset value R2*(0) estimated from preinjection R2* measurements in the same animal. ROIs were drawn to encompass the entire volume of normal liver parenchyma in each section while excluding nonhepatic tissues. These

ROIs were drawn for all sections in each animal for complete volumetric three-dimensional liver coverage. A whole-liver yttrium microsphere measurement for each animal was produced by a summation of these concentration values multiplied by the voxel size.

Statistical Analysis

Pearson correlation coefficients were calculated to compare known yttrium microsphere concentrations (according to phantom composition) to subsequent R2*-based microsphere concentration measurements in the phantom models. For in vivo studies, analysis of variance methods were used to evaluate between-group differences for R2*-based yttrium microsphere measurements with an assumption of randomized dose group experiments. An intraclass correlation was used to evaluate the consistency between the measured microsphere quantity and the dose of microspheres administered in each animal via transcatheter infusion. These analyses were implemented with Stata software (Stata-SE 13.1, Stata, College Station, Tex). $P < .05$ was considered to indicate a statistically significant difference.

Results

Phantom Studies

T2*-weighted images of phantom models showed a decreasing signal intensity with increases in SPIO-labeled yttrium microsphere concentration (Fig E1a and E1b [online]). The signal-to-noise ratios were found to decrease with the concentrations of the microspheres for all the four compositions of SPIO (Fig E1c [online]). For microspheres with 5%, 10%, and 20% SPIO, the measured R2* dropped until concentrations produced T2*-weighted signal reductions R2* values beyond an upper limit threshold (Fig E1d [online]). For microspheres with 5% and 10% SPIO, the highest R2* values were found at concentration of 8 mg/mL, while the peak R2* was found at 4 mg/mL for microspheres with 20% SPIO. A linear relationship was found across all seven concentrations for 2% SPIO yttrium microspheres (blue line in

Fig E1d [online]). Pearson correlation analysis showed a strong correlation ($R^2 = 1.00$, $P < .001$) between measured R2* and 2% SPIO yttrium microspheres across all seven concentrations. The mean calculated r2* relaxivity for 2% SPIO yttrium microspheres was 30.80 sec^{-1}·mg^{-1}·mL ± 0.23 (standard deviation). The mean r2* values for yttrium microsphere compositions of 5%, 10%, and 20% SPIO, determined from concentrations resulting in R2* less than the measured corresponding extrema, were 86.25 sec^{-1}·mg^{-1}·mL ± 2.57 (calculated from six SPIO concentrations: 0, 0.25, 0.5, 1.0, 2.0, 4.0, and 8.0 mg/mL), 94.72 sec^{-1}·mg^{-1}·mL ± 2.03 (calculated from six SPIO concentrations: 0, 0.25, 0.5, 1.0, 2.0, 4.0, and 8.0 mg/mL), and 167.05 sec^{-1}·mg^{-1}·mL ± 6.63 (calculated from five SPIO concentrations: 0, 0.25, 0.5, 1.0, 2.0, and 4.0 mg/mL), respectively.

Animal Model Studies

Representative in vivo and ex vivo T2-weighted images are shown in Figure 1a–1c, each acquired after infusion of yttrium microspheres containing 5% SPIO. Microspheres were heterogeneously distributed within the rat liver (Fig 1b). Signal voids in and surrounding blood vessels were found in T2-weighted images. SPIO-labeled microsphere deposition commonly produced characteristic dipole patterns (Fig 1c). Histologic analysis (Fig 1d) verified microsphere deposits in liver and aggregated clusters. Strong signal voids were found in T2-, T1-, and proton density–weighted images even with SPIO composition of only 2% (Fig 2a–2c). As expected, greater signal loss was found in tissues after infusions with microspheres of increased SPIO content, as shown in Figure 2c–2f. SPIO-labeled microspheres were heterogeneously distributed for each of the four different labeling compositions.

Figure 3 shows representative examples of coronal T2*-weighted images with color-coded overlays depicting voxelwise estimates of intrahepatic microsphere concentrations. Heterogeneous distribution patterns were observed in each of the concentration maps (Fig 3). After infusion of 5-, 10-, 15-, and
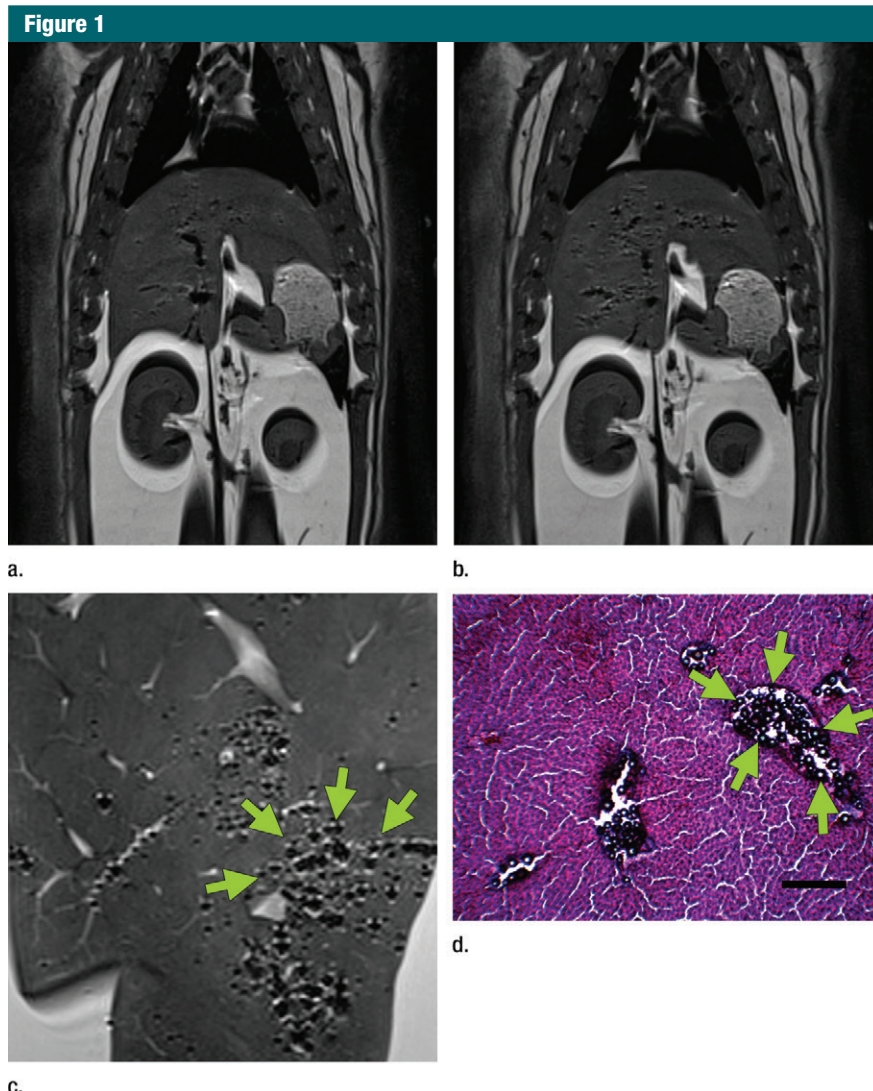
Figure 1

Figure 1: **(a–c)** T2-weighted MR images show the distribution of 5% SPIO-labeled yttrium microspheres **(a)** before infusion, **(b)** after infusion, and **(c)** ex vivo (high-resolution image). **(d)** Hematoxylin-eosin stained liver tissue shows microspheres (arrows). Scale bar = 0.5 mm. Arrows in **c** = microsphere deposition.

20-mg doses, the mean measured yttrium microsphere contents using R2* methods were 7.65 mg ± 1.90, 12.51 mg ± 2.19, 16.43 mg ± 1.02, and 21.08 mg ± 0.79, respectively (Fig 4). One-way analysis of variance indicated significant differences between intrahepatic R2* measurements for the four different groups ($P \leq .001$). MR imaging–based intrahepatic R2* measurements significantly increased with increased transcatheter yttrium microsphere dose, as indicated by a significant linear trends ($P \leq .001$). Comparison of MR imaging–based intrahepatic R2* measurements and the transcatheter-infused yttrium microsphere dose indicated intraclass correlation coefficients of 0.98 ($P < .001$, Fig 4).

Discussion

The clinical ability to quantify intrahepatic ^{90}Y microsphere deposition would permit dose optimization to maximize tumor kill and also potentially early prediction of longitudinal treatment outcomes. Response assessment with conventional cross-sectional imaging typically requires waiting several months postprocedure. In our preclinical study, we found that yttrium microspheres labeled with relatively low SPIO content (2% by mass) could be quantitatively detected with MR imaging at clinically relevant dose ranges (those anticipated when performing radioembolization using 3-GBq dose vials of glass ^{90}Y microspheres) (14).

Optimization of SPIO content in ^{90}Y microspheres may be critical to permit quantitative in vivo assessments of biodistribution. Microspheres with deficient SPIO content may not be visible with MR imaging, while those with excessive SPIO content rapidly reduce MR imaging signal even in proton density weighted images. Additionally, the heterogeneous deposition of the microspheres in liver tissue may lead to local-regional areas with high microsphere densities. Thus, the optimal microsphere composition must provide a wide concentration range that exhibits a relatively linear relationship between resulting MR imaging R2* measurements and microsphere content.

Previous liver explant studies found that within viable hypervascular tumor tissues, upwards of 254 glass ^{90}Y microspheres could be located within 1 mm^3 of tissue (4). We referred to this information to calculate the anticipated maximum concentration of SPIO-labeled microspheres, and extended the approximate maximum density to 800 spheres/mm^3 for our phantom studies to cover the possible extremities of local microsphere doses. For 2% microspheres, a monotonic and relatively linear relationship was maintained up to concentrations of 16 mg/mL (approximately 800 spheres per cubic millimeter) producing an R2* of roughly 500 sec^{-1}; quantification of even higher densities may be possible but it is unclear if such concentrations would occur in vivo. Similar monotonic, linear relationships were found between R2* measurements and microsphere concentrations for 5% and 10% SPIO compositions up to dose concentrations of 8 mg/mL (roughly 400 spheres per cubic millimeter). Considering that the current rodent studies were performed
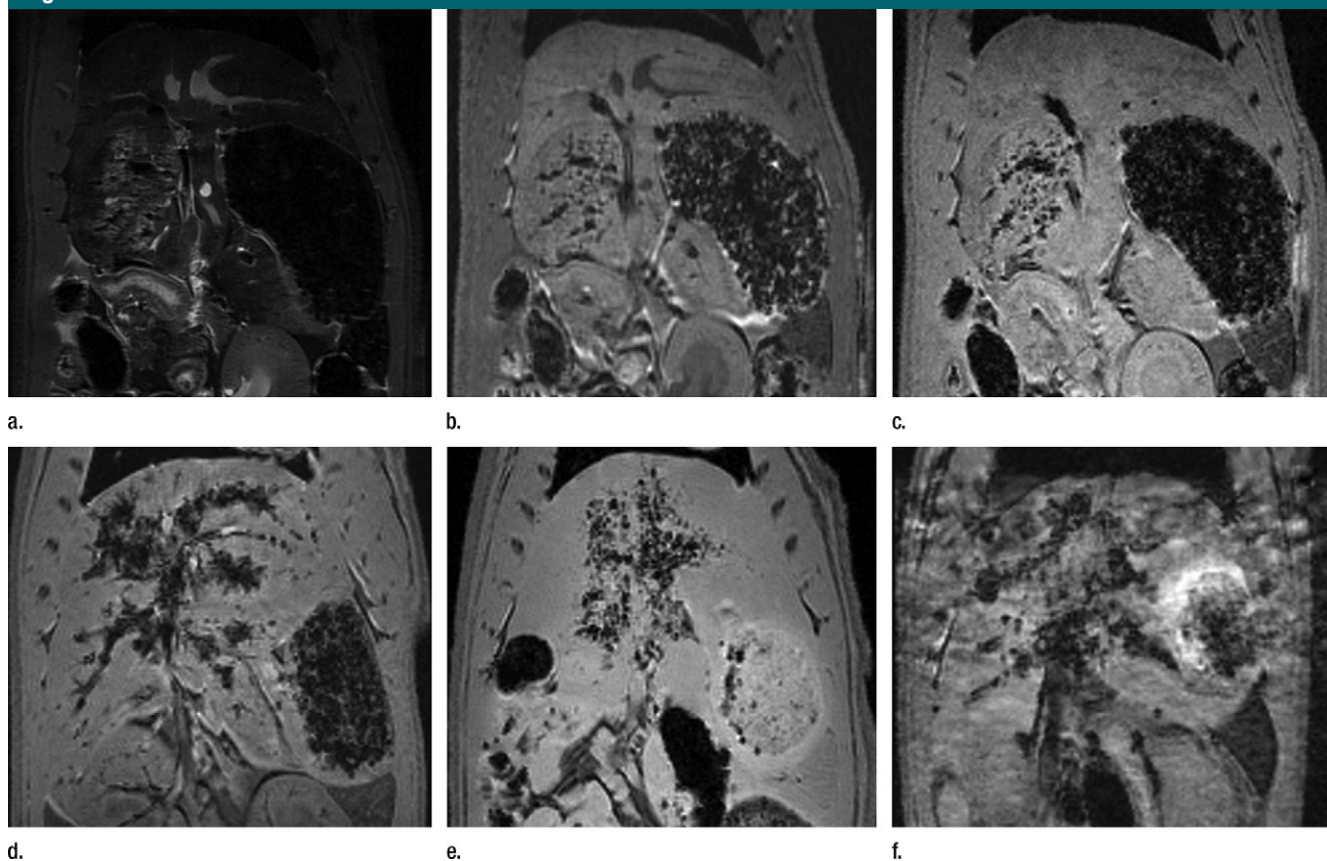
Figure 2

Figure 2: **(a–c)** Upper row shows distribution of 2% SPIO-labeled yttrium microspheres (5 mg infused) on **(a)** T2-weighted, **(b)** T1-weighted, and **(c)** proton density–weighted images. **(d–f)** Lower row shows proton density–weighted images in separate animals after infusion of 5 mg of yttrium microspheres with **(d)** 5%-, **(e)** 10%-, and **(f)** 20%-by-mass SPIO labeling.

at a high magnetic field strength (7.0 T), and given that susceptibility effects are smaller at lower magnetic field strengths (15), it is possible that these alternative compositions could also prove effective for quantitative imaging in clinical settings (1.5–3.0 T). However, after radioembolization in clinical settings, the delivered microspheres permanently remain in the tumor tissue even after devitalization. With shrinkage of large tumors or irradiated normal liver, the concentration of microspheres could be dramatically increased during follow-up with resulting MR artifacts thus impacting the accuracy of R2* measurements. Further optimization studies will clearly be required upon clinical translation.

The biodistribution of ^{90}Y microspheres can be evaluated by alternative methods such as PET/CT and SPECT/CT (6,11). However, the latter approaches provide rather poor anatomic soft-tissue contrast, and the spatial resolution provided by SPECT and PET is generally quite inferior to that of MR imaging. Also PET and SPECT are not part of the standard of care after ^{90}Y administration, whereas almost all of these patients undergo follow-up MR imaging. However, studies will be necessary to compare the performance of MR imaging R2* measurements of SPIO-labeled ^{90}Y microspheres with that of currently imaging modalities such as SPECT/CT or PET/CT at the clinical settings. A clear limitation of our SPIO-labeled microsphere approach is that quantitative evaluation pulmonary shunt fraction may prove infeasible due to magnetic susceptibility artifacts at air-tissue interfaces during MR imaging of the lung. Conventional [99 m]Tc-MAA scans would likely remain necessary for this purpose.

One important limitation of our study is that the relaxivity of microspheres in homogeneous gel phantoms may not apply directly to in vivo heterogeneous and structured biodistributions. The exact quantitative relationship between relaxivity and biodistribution is difficult to predict. Alignment of the SPIO-labeled microsphere dose along a large vessel might cause main magnetic field distortion. Furthermore, static and radiofrequency field inhomogeneity, section profile effects, as well as diffusion effects and air-tissue interfaces, can affect R2* measurements (16). Excessive signal loss by these effects could be falsely interpreted as being related to microsphere
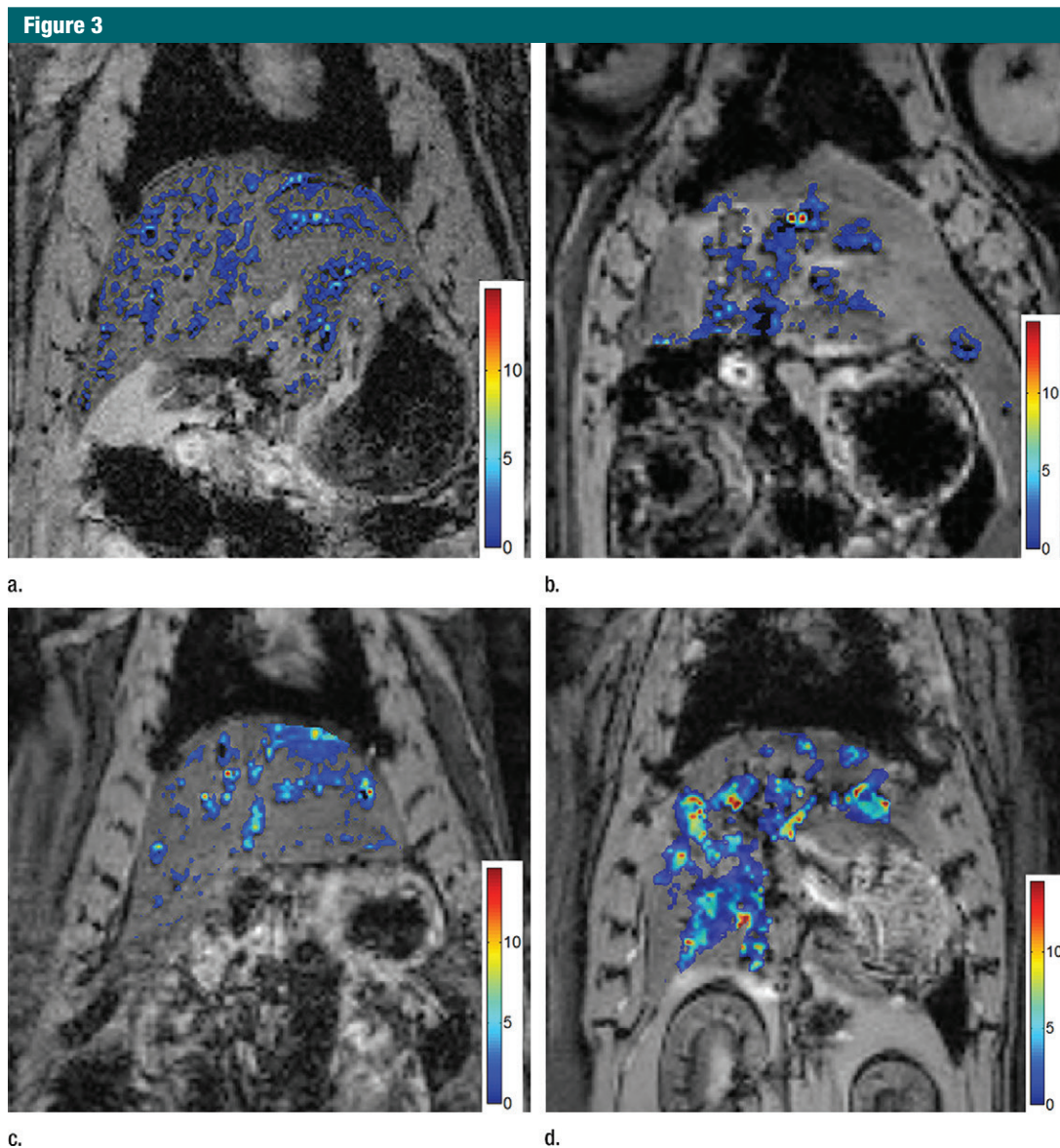
Figure 3: (a–d) Coronal T2*-weighted MR images with color-coded overlays depicting voxelwise estimates of intrahepatic microsphere concentrations. Representative examples are shown for different rodents after infusions of **(a)** 5-mg, **(b)** 10-mg, **(c)** 15-mg, and **(d)** 20-mg doses of 2% SPIO-labeled yttrium microspheres. Color bar unit: milligrams per milliliter.

uptake during R2* measurements, thus leading to an overestimation of the local concentration of microspheres. In practice, attention should be made to calibrate the overall local field inhomogeneity effects to obtain accurate quantification results. For our in vivo qualitative measurements, 5 mg of yttrium microspheres with four compositions of SPIO were administrated to rat livers through the portal vein. Ambiguous

signal losses and an expected increase in signal loss were found in tissues infused with microspheres having greater SPIO content. Despite the heterogeneity of the microsphere distribution, R2* measurements for livers infused with yttrium microspheres of 2% SPIO indicated a significant linear trend with respect to the infused microsphere dose. However, we noticed that the standard deviation of these R2* measurements

was markedly larger for group 1 and two animals that were infused with 5 and 10 mg of 2% SPIO-labeled YAS microspheres, respectively. This larger deviation may have been the result of different biodistributions for the rodents in groups 1 and 2 as opposed to the biodistribution in groups 3 and 4 that received larger microspheres doses. Further studies are necessary to confirm and elucidate the source(s) of this
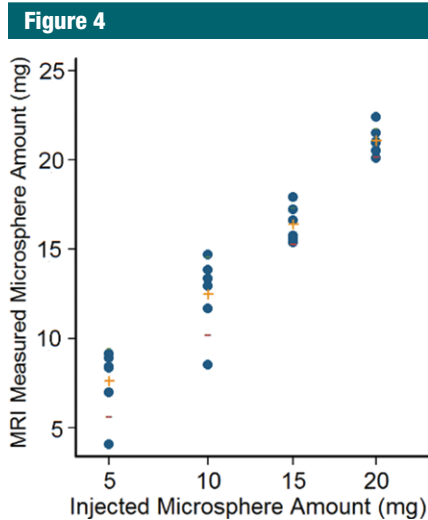
Figure 4

Figure 4: Graph shows results of comparison between transcatheter-infused SPIO-labeled yttrium microsphere doses (2% SPIO composition) and the resulting MR imaging R2*–based measurements of intrahepatic microsphere delivery. Solid lines = upper and lower quartiles. Hatched lines = mean values.

increased measurement variability. One additional limitation was that the portal vein rather than the hepatic artery was used for infusion in these rodent model studies. Our rationale for this approach was that hepatic arterial infusion remains a highly delicate procedure in rodents because of the small anatomic size of these vessels. For our study intending to broadly distribute the microspheres to normal hepatic parenchyma, intra-arterial infusions may be unnecessary because these rodents did not have implanted tumors (with associated arterial supply). However, further studies remain necessary to confirm the accuracy of our proposed MR imaging methods monitoring distributions and/or intratumoral delivery following hepatic arterial injections as typically performed in clinical settings. Several additional limitations included the investigation of only four glass microsphere compositions (2%-, 5%-, 10%-, and 20%-by-mass SPIO microspheres) and an animal model without tumors; additional studies with broader range of microsphere compositions and carrier materials (eg, resin) and primary or metastatic liver tumor models will be value to inform clinical translation.

In conclusion, our studies demonstrated that MR imaging R2* measurements of SPIO-labeled yttrium microspheres can quantitatively depict in vivo intrahepatic biodistributions in the rat model. Once translated into clinical settings, these methods should permit early predictions radioembolization outcomes based upon the observed biodistribution of the microspheres.

Practical application: Our study found that MR imaging R2* measurements of yttrium microspheres labeled with 2% SPIO offer the potential to quantitatively depict in vivo intrahepatic biodistributions. Our study demonstrated the potential to optimize SPIO content for future studies intending to quantify intrahepatic ⁹⁰Y microsphere delivery in clinical settings.

References

1. El-Serag HB. Hepatocellular carcinoma. N Engl J Med 2011;365(12):1118–1127.

2. Jemal A, Bray F, Center MM, Ferlay J, Ward E, Forman D. Global cancer statistics. CA Cancer J Clin 2011;61(2):69–90.

3. Salem R, Thurston KG, Carr BI, Goin JE, Geschwind JF. Yttrium-90 microspheres: radiation therapy for unresectable liver cancer. J Vasc Interv Radiol 2002;13(9 Pt 2):S223–S229.

4. Campbell AM, Bailey IH, Burton MA. Analysis of the distribution of intra-arterial microspheres in human liver following hepatic yttrium-90 microsphere therapy. Phys Med Biol 2000;45(4):1023–1033.

5. Salem R, Thurston KG. Radioembolization with 90yttrium microspheres: a state-of-the-art brachytherapy treatment for primary and secondary liver malignancies. Part 2: special topics. J Vasc Interv Radiol 2006; 17(9):1425–1439.

6. Mansberg R, Sorensen N, Mansberg V, Van der Wall H. Yttrium 90 Bremsstrahlung SPECT/CT scan demonstrating areas of tracer/tumour uptake. Eur J Nucl Med Mol Imaging 2007;34(11):1887.

7. Tehranipour N, Al-Nahhas A, Canelo R, et al. Concordant F-18 FDG PET and Y-90 Bremsstrahlung scans depict selective delivery of Y-90-microspheres to liver tumors: confirmation with histopathology. Clin Nucl Med 2007;32(5):371–374.

8. Ho S, Lau WY, Leung TW, et al. Tumour-to-normal uptake ratio of 90Y microspheres in hepatic cancer assessed with 99Tcm macroaggregated albumin. Br J Radiol 1997; 70(836):823–828.

9. Hung JC, Redfern MG, Mahoney DW, Thorson LM, Wiseman GA. Evaluation of macroaggregated albumin particle sizes for use in pulmonary shunt patient studies. J Am Pharm Assoc (Wash) 2000;40(1):46–51.

10. Gates VL, Esmail AA, Marshall K, Spies S, Salem R. Internal pair production of 90Y permits hepatic localization of microspheres using routine PET: proof of concept. J Nucl Med 2011;52(1):72–76.

11. Kao YH, Tan EH, Ng CE, Goh SW. Yttrium-90 time-of-flight PET/CT is superior to Bremsstrahlung SPECT/CT for postradioembolization imaging of microsphere biodistribution. Clin Nucl Med 2011;36(12):e186–e187.

12. Lhommel R, Goffette P, Van den Eynde M, et al. Yttrium-90 TOF PET scan demonstrates high-resolution biodistribution after liver SIRT. Eur J Nucl Med Mol Imaging 2009; 36(10):1696.

13. Gupta T, Virmani S, Neidt TM, et al. MR tracking of iron-labeled glass radioembolization microspheres during transcatheter delivery to rabbit VX2 liver tumors: feasibility study. Radiology 2008;249(3):845–854.

14. Gray BN, Anderson JE, Burton MA, et al. Regression of liver metastases following treatment with yttrium-90 microspheres. Aust N Z J Surg 1992;62(2):105–110.

15. Farahani K, Sinha U, Sinha S, Chiu LC, Lufkin RB. Effect of field strength on susceptibility artifacts in magnetic resonance imaging. Comput Med Imaging Graph 1990; 14(6):409–413.

16. Seppenwoolde JH, Nijsen JF, Bartels LW, Zielhuis SW, van Het Schip AD, Bakker CJ. Internal radiation therapy of liver tumors: qualitative and quantitative magnetic resonance imaging of the biodistribution of holmium-loaded microspheres in animal models. Magn Reson Med 2005;53(1):76–84.